Geomechanics and Engineering, *Vol. 5, No. 5 (2013) 379-399*
DOI: http://dx.doi.org/10.12989/gae.2013.5.5.379

Winkler Springs (*p-y* curves) for pile design from stress-strain of soils: FE assessment of scaling coefficients using the Mobilized Strength Design concept

Dj. Amar Bouzid[*1] S. Bhattacharya[2] and S.R. Dash[3]

[1] *Department of Civil Engineering, Faculty of Sciences and Technology, University of Médéa, Quartier Ain D'hab, Médéa 26000, Algeria*
[2] *Department of Civil Engineering, University of Bristol, Room 237, Queens Building, Bristol BS8 1TR, UK*
[3] *Department of Civil Engineering, Indian Institute of Technology, Bhubaneswar, India*

(Received November 29, 2012, Revised April 28, 2013, Accepted May 08, 2013)

Abstract. In practice, analysis of laterally loaded piles is carried out using beams on non-linear Winkler springs model (often known as *p-y* method) due to its simplicity, low computational cost and the ability to model layered soils. In this approach, soil-pile interaction along the depth is characterized by a set of discrete non-linear springs represented by *p-y* curves where *p* is the pressure on the soil that causes a relative deformation of *y*. *p-y* curves are usually constructed based on semi-empirical correlations. In order to construct API/DNV proposed *p-y* curve for clay, one needs two values from the monotonic stress-strain test results i.e., undrained strength (s_u) and the strain at 50% yield stress (ε_{50}). This approach may ignore various features for a particular soil which may lead to un-conservative or over-conservative design as not all the data points in the stress-strain relation are used. However, with the increasing ability to simulate soil-structure interaction problems using highly developed computers, the trend has shifted towards a more theoretically sound basis. In this paper, principles of Mobilized Strength Design (MSD) concept is used to construct a continuous *p-y* curves from experimentally obtained stress-strain relationship of the soil. In the method, the stress-strain graph is scaled by two coefficient N_C (for stress) and M_C (for strain) to obtain the *p-y* curves. M_C and N_C are derived based on Semi-Analytical Finite Element approach exploiting the axial symmetry where a pile is modelled as a series of embedded discs. An example is considered to show the application of the methodology.

Keywords: semi-analytical FE analysis; MSD; *p-y* curves; interface elements; laterally loaded single piles; strain energy

1. Introduction

The behavior of laterally loaded piles is a complex soil structure interaction problem that has received a considerable amount of attention over the last four decades mainly in the field of offshore engineering or earthquake geotechnical engineering due to large stakes involved, see for example (Hajialilue-Bonab *et al*. 2011, Adhikari and Bhattacharya 2011). The primary function of a pile or a group of piles is to transfer the external loads from the superstructure to the surrounding soil medium without causing excessive deflections at the top of the pile or piles. The analysis of

*Corresponding author, Associate Professor, E-mail: d_amarbouzid@yahoo.fr

http://www.techno-press.org/?journal=gae&subpage=7 ISSN: 2005-307X (Print), 2092-6219 (Online)

such a problem is complicated because of the complex stress-strain behavior of the soil surrounding the piles. This problem could be solved rigorously using the 3D finite element (FE) or finite difference (FD) methods. However, the complexity of simulating the nonlinearities of the soil/pile interaction, the enormous effort of data preparation and the high computational cost render the 3-D FE analysis unfeasible and uneconomical for most cases. On the other hand, these rigorous methods can be used to validate the simplified easy-to-use Winkler spring models (also known as *p-y* methods) that are often employed in practice. The application and limitations of the Winkler spring model are discussed below.

The simplest and practical way to solve a laterally loaded pile is to adopt a generalized Winkler spring model with a load transfer function called *p-y* curve, which defines the relationship between the soil reaction *p* (load per unit length of pile, Unit: kN/m) and the lateral displacement *y* (Unit: mm) along the pile. A number of different methods are in use to construct the *p-y* curves including:

(a) Semi-empirical methods based on back analysis of field lateral load tests together with laboratory stress-strain curves obtained from triaxial tests, see for example (API 2001, DNV 2001, McClelland and Focht 1958, Reese *et al*. 1974, 2000, Bowles 1996, Cox *et al*. 1974, Reese and Impe 2001).

(b) Results from pressuremeter tests. The *p-y* curve, in this method is assumed to be directly related to the pressuremeter expansion curve (Bouafia 2007, Frank 2009).

Obviously the Winkler model (Fig. 1) cannot fully captures the 3D aspect of soils, but it offers a practical tool for analysis and design. The fundamental assumption on which the technique of constructing a *p-y* curve is based is the similarity between the load deformation pattern of pile head and the stress-strain behaviour of the interacting soil from carefully chosen element testing (e.g., triaxial tests). The transformation of stress-strain curve to *p-y* curve is schematically shown in Fig. 2 where three parameters are required: M_C, N_C and D (pile diameter). M_C and N_C are similar to the concept of Mobilizable Strength Design (MSD) proposed by Osman and Bolton (Osman and Bolton 2005). At the depth considered, the behaviour of the soil-pile system is assumed to satisfy plane strain conditions. The pile, which is represented by a stack of circular discs in the analysis, is assumed to be rigid.

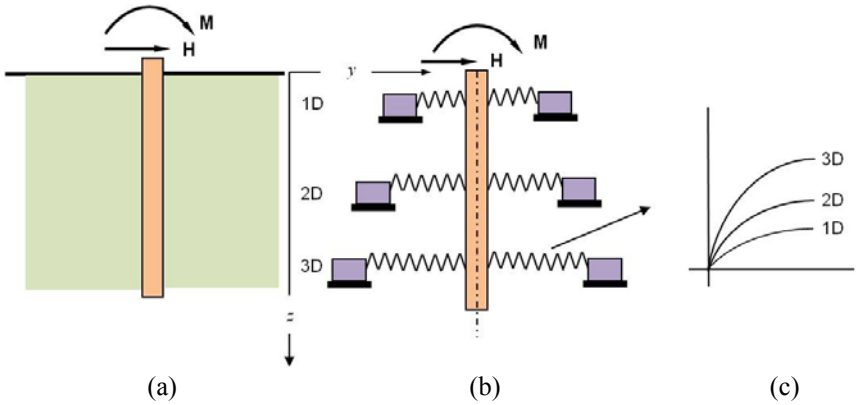

Fig. 1 Single pile under lateral loading: (a) real vertical pile; (b) Winkler idealization; (c) *p-y* curves for lateral Winkler springs

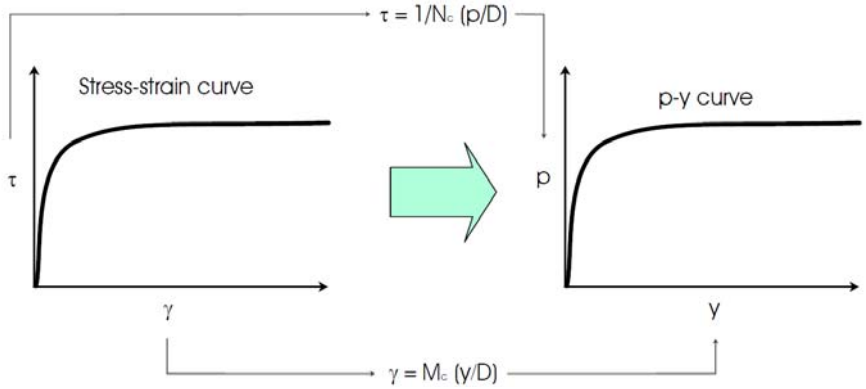

Fig. 2 Schematic figure showing the procedure of obtaining *p-y* curve from stress-strain behaviour. Note M_C and N_C are the scaling coefficients to convert the stress-strain to *p-y*

Non-linear Winkler springs or *p-y* curves for sand (under non-liquefied condition), soft clay, and stiff clay are available, see for example API (2001) or DNV code (DNV 2001). These standardised curves are semi-empirical and are well calibrated for offshore applications. However non-standardised soils (i.e., mixed soils which are not strictly sand or clay, intermediate soils, partially liquefied soil or fully liquefied soils) are often encountered in practice and in such cases *p-y* curves need to be derived from stress-strain characteristics of the soil.

Fig. 3 shows the stress strain relationship for Bothkennar clay obtained from high quality stress-path cell at the University of Bristol. Fig. 4 shows the construction of *p-y* curve using API method which uses two values from the stress-strain graph:

(a) Undrained strength (31 kPa for this case);
(b) Strain which occurs at 50% failure stress in a laboratory undrained compression test denoted by ε_{50} which is 0.11% for the case considered here.

It is recognized that the development of lateral resistance on a pile (i.e., *p-y* curve) should bear

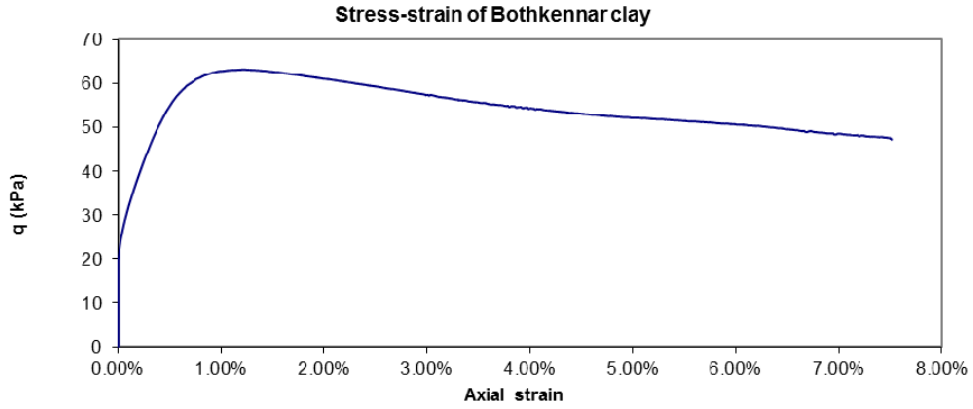

Fig. 3 Stress-strain data of Bothkennar clay obtained from triaxial tests

some resemblance to the stress-strain response in some laboratory shear test. Clearly, the *p-y* curve in this case does not capture the stress-strain characteristics in the sense that the high stiffness of the clay at small strain is not captured in the API formulation. As the determination of *p-y* curves relied mostly on empirical correlations, and with increasing ability to simulate problems using highly sophisticated computers, the trend has shifted towards a more theoretically sound basis. The objective of this paper is therefore to assess the transfer coefficients that allow to scale *p-y* curves starting from the stress-strain relationships determined experimentally in laboratory. The basic idea here comes from the fact that the shape of p-y curve is geometrically similar to the stress-strain curve of the soil material (Dash *et al*. 2008). This is, because the *p-y* curve is characterized by index properties of the soil and the pile dimensions. The index properties of the soil are basically a representation of its stress-strain behaviour. Semi-analytical Finite Element approach is employed here to find the parameters N_C and M_C (see Fig. 2) that permits scaling from stress-strain relationships to *p-y* curves.

As the methodology followed to obtain the parameters N_C and M_C is restricted to linear elasticity, these values can be employed to scale stress-strain curve to *p-y* curve till elastic zone. Other empirical values obtained from the literature are used in the fully plastic conditions. Furthermore, in laterally loaded piles analysis, this procedure has some limitations in the sense that this *p-y* curve is suited for a deeper depth and may be unrealistic in the top part of the pile due to the wedge mechanism that develops.

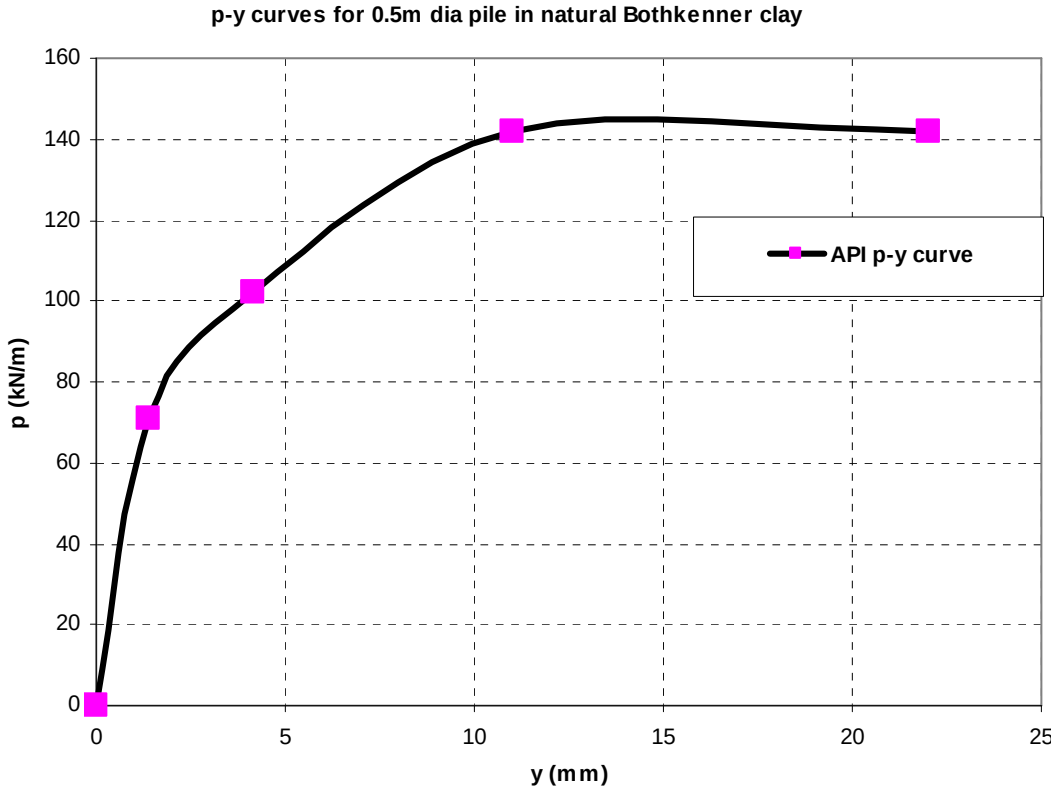

Fig. 4 *p-y* curve for a 0.5 m diameter pile using the API method

2. Statement of the problem and semi analytical FE formulation

A laterally loaded embedded disc is often taken as a representative model for the behavior of the soil around a short segment of a long pile under horizontal loading, well away from the effect of the tip and the ground surface. This model which occurs within a laterally loaded circular pile at sufficient depth below the ground level is often used to establish the *p-y* curves. The soil-pile interaction at a particular depth is considered (Fig. 5) with the following assumptions in the analysis.

(a) Pile deflection '*y*' is compatible with the strain distribution in the soil.

(b) The stresses in the soil are in equilibrium with the reaction force on pile '*p*'.

The basic idea comes from the fact that the loading on the soil is represented by a single pressure *p* which produces a single deformation *y*.

2.1 Description of strain and displacement fields

As the geometry of the pile-soil interaction is axisymmetric, it is convenient to adopt a cylindrical coordinate system for the semi-analytical FE formulation. The six strain components may be related to the three displacements components which are the radial displacement, u_r, the axial displacement v_z and the circumferential displacement w_θ. The strain formulation thus yields

$$\varepsilon_r = \frac{\partial u_r}{\partial r}, \quad \varepsilon_z = \frac{\partial v_z}{\partial z}, \quad \varepsilon_\theta = \frac{\partial w_\theta}{r\partial\theta} + \frac{u_r}{r} \tag{1}$$

$$\gamma_{rz} = \frac{\partial u_r}{\partial z} + \frac{\partial v_z}{\partial r}, \quad \gamma_{z\theta} = \frac{\partial v_z}{r\partial\theta} + \frac{\partial w_\theta}{\partial z}, \quad \gamma_{\theta r} = \frac{\partial u_r}{r\partial\theta} + \frac{\partial w_\theta}{\partial r} - \frac{u_r}{r} \tag{2}$$

Following the standard procedure of Fourier series representation (Cook *et al*. 2001) one can write

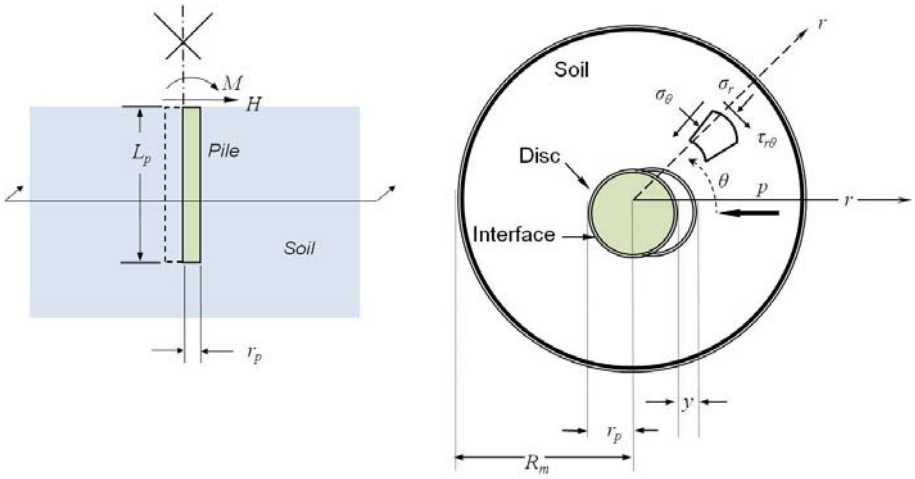

Fig. 5 Plane strain idealisation of pile-soil interaction at a particular depth of consideration

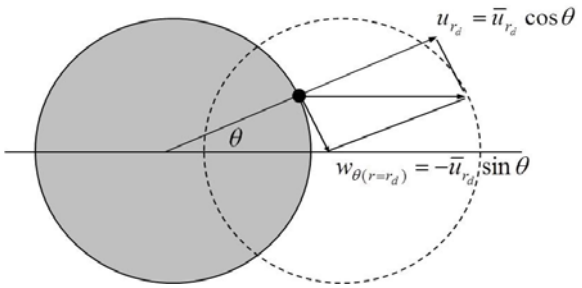

Fig. 6 Displacement components in radial coordinate

$$
\begin{aligned}
u_r &= \sum_{i=0}^{L} \overline{u}_{ri} \cos i\theta + \sum_{i=1}^{L} \overline{\overline{u}}_{ri} \sin i\theta \\
v_z &= \sum_{i=0}^{L} \overline{v}_{zi} \cos i\theta + \sum_{i=1}^{L} \overline{\overline{v}}_{zi} \sin i\theta \\
w_r &= \sum_{i=1}^{L} \overline{w}_{\theta i} \sin i\theta + \sum_{i=0}^{L} \overline{\overline{w}}_{\theta i} \cos i\theta
\end{aligned}
\tag{3}
$$

The index i stands for the harmonic number, and L is the total number of harmonic terms considered in the series. The single barred terms $\overline{u}_{ri}$, $\overline{v}_{zi}$, $\overline{w}_{\theta i}$ are amplitudes of displacements that are symmetric with respect to the plane for $\theta = 0$. The double barred terms $\overline{\overline{u}}_{ri}$, $\overline{\overline{v}}_{zi}$, $\overline{\overline{w}}_{\theta i}$ are the amplitudes of displacements that are antisymmetric with respect to the plane for $\theta = 0$.

Only the first two terms in the Fourier series are needed in most practical situations. Problems for the first term (i.e., $i = 0$) are those related to purely axisymmetric problems and consequently well established in the literature. The second term for $i = 1$ is required when the loading pattern has a plane of symmetry. In this situation the components of displacement will reduce to

$$
u_r = \overline{u}_r \cos\theta, \quad v_z = \overline{v}_z \cos\theta, \quad w_\theta = \overline{w}_\theta \sin\theta \tag{4}
$$

The strains and stresses calculated at the Gauss points are themselves amplitudes. The actual values of stresses at various tangential locations are therefore found from the relationships

$$
\begin{aligned}
\sigma_r &= \overline{\sigma}_r \cos\theta, \quad \tau_{rz} = \overline{\tau}_{rz} \cos\theta \\
\sigma_z &= \overline{\sigma}_z \cos\theta, \quad \tau_{r\theta} = \overline{\tau}_{r\theta} \sin\theta \\
\sigma_\theta &= \overline{\sigma}_\theta \cos\theta, \quad \tau_{\theta r} = \overline{\tau}_{\theta r} \sin\theta
\end{aligned}
\tag{5}
$$

Where, the barred terms are the computed amplitudes. Similar expressions exist for the six components of strain. Although more work and storage are required than for a true 2D analysis, the fact that finite element discretisation is only required in radial plane means that band-width problems that occur with 3D elements are avoided. Thus the problem is easier for the analyst and is less demanding when considering computer resources.

2.2 Interface elements

In most problems of soil-structure interaction, relatively simple models may be adopted for

interfaces as they usually involve compressive contact stresses. For many problems it may be convenient to model interface behavior by merely refining a finite element mesh in the immediate vicinity of the interface. However, as the mesh remains continuous and adjacent elements are assigned with considerably different properties, occasional numerical singularities may occur constituting thus, the main drawback of this simple method.

A joint element was thus formulated by Amar Bouzid *et al*. (2004) and Amar Bouzid (2011) to model soil/structure interfaces of axisymmetric solids of revolution subjected to non-axisymmetric loading using a semi-analytical analysis. To this end a six-noded interface element was formulated which can be combined with eight or nine-noded quadrilateral volume elements (Fig. 7). A brief outline of the interface formulation will be given here.

According to the standard formulation of the displacement-based finite element method (Zienkiewicz and Taylor 1991), the stiffness matrix K_{int} of the interface element is given by the equation

$$K_{\text{int}} = \int_A B^T D\, B\, dA \tag{6}$$

Where, B is the strain-displacement matrix, D is the constitutive matrix and A is the area of the interface element. The thickness of the interface element is taken to be zero.

Since the interface element is a fictive location and is not a material itself, it represents only the interaction between two dissimilar materials. Hence, there will exist only a normal stress, σ_{ni}, and shear stresses, τ_{sni} and $\tau_{n\theta i}$, in this imaginary area. The displacement-stress relationships can be written as

$$\sigma_i = D\, u_{rel} \tag{7}$$

where, $\sigma_i = \begin{Bmatrix} \tau_{sni} \\ \sigma_{ni} \\ \tau_{n\theta i} \end{Bmatrix}$, $D = \begin{bmatrix} k_s & 0 & 0 \\ 0 & k_n & 0 \\ 0 & 0 & k_s \end{bmatrix}$ and $u_{rei} = B\,\overline{u}^e$.

The interface shear stiffness k_s and the interface normal stiffness k_n are in units of force per cube length. The vector of radial, axial and circumferential nodal displacement amplitudes in the

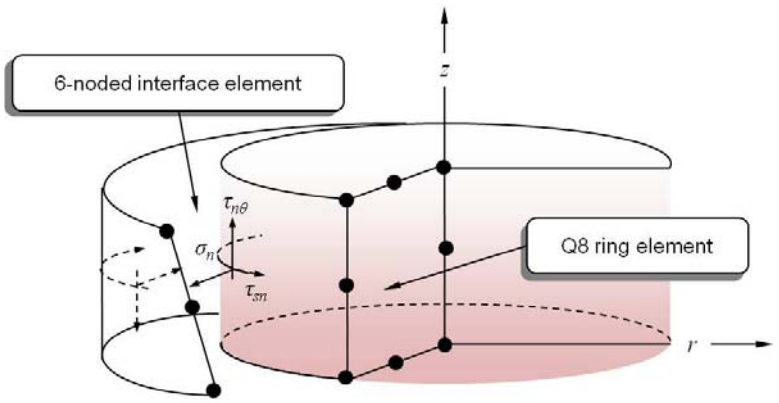

Fig. 7 Zero thickness 6-noded interface element in an axisymmetric body showing the normal and shear stresses acting at the interface location

global coordinate system can be written as $\overline{u}^e = [\overline{u}_1, \overline{v}_1, \overline{w}_1, \ldots \ldots, \overline{u}_6, \overline{v}_6, \overline{w}_6]^T$. As most interface stiffness matrices have been based on numerical integration, the present analytical formulation has the advantage to avoid spurious oscillations of stresses over interface area as it is accurately determined.

3. Significance of the transfer coefficients M_C and N_C using of the mobilized shear strength design concept

Osman and Bolton (2005) have proposed an interesting technique, called Mobilised Strength Design (MSD), for the evaluation of soil response to the structure loading in terms of load-deformation behaviour. The key feature of the MSD is that a single stress and a single strain are chosen to represent the behaviour of the soil mass under any given loading conditions. The representative stress is related to the applied load, and the representative strain is related to the applied displacement. If a stress-strain relationship is known for the soil, then this can be converted to an equivalent load-displacement relationship for the chosen problem.

Clearly the MSD approach cannot be expected to describe the detailed response with great accuracy, as a number of approximations are involved, most importantly.

(a) A single stress value cannot represent the stress state of the entire soil mass.
(b) Likewise a single strain state cannot represent the strains in an entire soil mass.

Nevertheless, as demonstrated by Osman and Bolton, the approach lies within the tradition of robust engineering applications for two fundamental reasons: firstly, the MSD can provide a realistic estimate of load-deformation behaviour, and secondly, it has the very significant benefit that no very complex calculations are needed. These authors proposed a simple plasticity method for the prediction of undrained settlement of shallow foundations in a clayey soil. In principle, their problem is similar to the problem of laterally loaded piles, as they also searched for a relationship between a load on a foundation and the settlement (which is a vertical displacement). The definitions of M_C and N_C are illustrated in Fig. 2.

3.1 FE evaluation of the mobilized shear strain

The soil-pile interaction at a particular depth is represented by a plane strain 2D model. Assuming the soil and pile are initially in equilibrium, any incremental work done by pile movement is equal to the total stain energy in the system. The pile is considered as very rigid with respect to soil, so that all the strain energy is assumed to be in the soil.

The engineering shear strain ε_s can be defined as the difference between the major and the minor principal strains

$$\varepsilon_s = \varepsilon_1 - \varepsilon_3 \tag{8}$$

Following Osman and Bolton, the average shear strain mobilized in the deforming soil can be calculated from the spatial average of the shear strain in the whole volume of the deformation zone. This mobilized shear strain can be associated with the pile displacement as follows

$$\varepsilon_{s,mob} = \frac{\int_v \varepsilon_s dv}{\int_v dv} \tag{9}$$

As the semi-analytical FE approach is used in this paper, the Eq. (9) can be re-written as

$$\varepsilon_{s,mob} = \frac{\int_v \varepsilon_s dv}{\int_v dv} = \frac{\int_v \sqrt{(\varepsilon_r - \varepsilon_\theta)^2 + \gamma_{\theta r}^2}\, dv}{\int_v dv} \tag{10}$$

where, $\varepsilon_s = \varepsilon_1 - \varepsilon_3 = \sqrt{(\varepsilon_r - \varepsilon_\theta)^2 + \gamma_{\theta r}^2}$.

The strain components are expressed in the circumferential direction with cosine and sine functions. Hence, the maximum shear strain will have the following form in terms of amplitudes

$$\sqrt{(\varepsilon_r - \varepsilon_\theta)^2 + \gamma_{\theta r}^2} = \sqrt{(\bar{\varepsilon}_r - \bar{\varepsilon}_\theta)^2 \cos^2\theta + \bar{\gamma}_{\theta r}^2 \sin^2\theta} \tag{11}$$

where, the barred terms are amplitudes. Some algebraic manipulations will lead to the following equation

$$\varepsilon_s = \left|\bar{\varepsilon}_r - \bar{\varepsilon}_\theta\right| \sqrt{1 - \lambda \sin^2\theta} \tag{12}$$

where, $\lambda = 1 - \dfrac{\gamma_{\theta r}^2}{(\bar{\varepsilon}_r - \bar{\varepsilon}_\theta)^2}$.

In integrating Eq. (12) we are facing an elliptic integral of second kind for which it is difficult to obtain a closed form solution. In order to overcome this problem and to compute the mobilized shear strain two cases should be considered

Case I

$0 < \dfrac{\gamma_{\theta r}^2}{(\bar{\varepsilon}_r - \bar{\varepsilon}_\theta)^2} < 1$. Since $\lambda < 1$ in this case, it is possible to put $\lambda = k^2 = \sin^2\alpha$, where $k = \sqrt{\lambda}$.

The expression of the mobilized shear strain becomes

$$\varepsilon_{s,mob} = \frac{\int \left|\bar{\varepsilon}_r - \bar{\varepsilon}_\theta\right| \sqrt{1 - \lambda \sin^2\theta}\, dv}{\int dv} = \frac{1}{\pi(R_m^2 - r_d^2)} \int_{-1}^{1}\int_{-1}^{1} \left|\bar{\varepsilon}_r - \bar{\varepsilon}_\theta\right| \int_0^{2\pi} \sqrt{1 - k^2 \sin^2\theta}\, r\, d\xi\, d\eta\, d\theta\, |J| \tag{13}$$

where, $|J|$ is the determinant of the Jacobian matrix.

Because the root function is positive and periodic of $\pi/2$, the integral with respect to the circumferential direction can be evaluated as

$$\int_0^{2\pi} \sqrt{1 - k^2 \sin^2\theta}\, d\theta = 4 \int_0^{\pi/2} \sqrt{1 - k^2 \sin^2\theta}\, d\theta \tag{14}$$

The integral $\int_0^{\pi/2} \sqrt{1 - k^2 \sin^2\theta}\, d\theta$ is called complete elliptic integral of second kind symbolized by $E(k)$, where k stands for the modulus and $\pi/2$ is the amplitude. There is no closed form solution for this integral. However, an approximate solution has been found (Byrd and Friedman 1971)

$$\int_0^{\pi/2} \sqrt{1-k^2\sin^2\theta}\,d\theta = \frac{\pi}{2}\left(1-\frac{1}{4}k^2-\frac{3}{64}k^4-\frac{5}{256}k^6-\frac{175}{16384}k^8-\frac{441}{65536}k^{10}-\cdots\right) \quad (15)$$

So, the final expression of the mobilized shear strain (Eq. (13)) will be

$$\varepsilon_{s,mob} = \frac{2}{R_m^2-r_d^2}\int_{-1}^{1}\int_{-1}^{1}\left|\bar{\varepsilon}_r-\bar{\varepsilon}_\theta\right|\left(1-\frac{1}{4}k^2-\frac{3}{64}k^4-\frac{5}{256}k^6-\frac{175}{16384}k^8-\cdots\right) r\,d\xi\,d\eta\,|J| \quad (16)$$

Case II

$\frac{\gamma_{\theta r}^2}{(\bar{\varepsilon}_r-\bar{\varepsilon}_\theta)^2} > 1$. In this case λ becomes negative, and the integral of the function (12) is no longer elliptic in this form. In this situation, it is possible to re-write Eq. (12) in a different way

$$\varepsilon_s = |\bar{\gamma}_{\theta r}|\sqrt{1-\delta\cos^2\theta} \quad (17)$$

where, $\delta = 1-\frac{(\bar{\varepsilon}_r-\bar{\varepsilon}_\theta)^2}{\gamma_{\theta r}^2}$. Here δ is less than 1.

Eq. (17) can be written as

$$\varepsilon_s = |\bar{\gamma}_{\theta r}|\sqrt{1-\delta\cos^2\theta} = \frac{|\bar{\gamma}_{\theta r}|}{\sqrt{2}}\sqrt{1+\left(\frac{(\bar{\varepsilon}_r-\bar{\varepsilon}_\theta)}{\bar{\gamma}_{\theta r}}\right)^2}\sqrt{1-\Delta\cos(2\theta)} \quad (18)$$

where, $\Delta = 1-\left(\frac{(\bar{\varepsilon}_r-\bar{\varepsilon}_\theta)}{\bar{\gamma}_{\theta r}}\right)^2 \Big/ 1+\left(\frac{(\bar{\varepsilon}_r-\bar{\varepsilon}_\theta)}{\bar{\gamma}_{\theta r}}\right)^2$.

Now the integral of the third term in Eq. (18) over a quarter of the circumference is a complete elliptic integral of second kind. Hence

$$\int_0^{\pi/2}\sqrt{1-\Delta\cos(2\theta)}\,d\theta = \sqrt{1+\Delta}\;\; E\left(\frac{\pi}{2},\sqrt{\frac{2\Delta}{1+\Delta}}\right) \quad (19)$$

So Eq. (9) becomes

$$\varepsilon_{s,mob} = \frac{4}{\pi(R_m^2-r_d^2)}\int_{-1}^{1}\int_{-1}^{1}|\bar{\gamma}_{\theta r}|\,E\left(\frac{\pi}{2},\sqrt{1-\left(\frac{(\bar{\varepsilon}_r-\bar{\varepsilon}_\theta)}{\bar{\gamma}_{\theta r}}\right)^2}\right) r\,d\xi\,d\eta\,|J| \quad (20a)$$

$$\varepsilon_{s,mob} = \frac{2}{(R_m^2-r_d^2)}\int_{-1}^{1}\int_{-1}^{1}|\bar{\gamma}_{\theta r}|\left(1-\frac{1}{4}k^2-\frac{3}{64}k^4-\frac{5}{256}k^6-\frac{175}{16384}k^8-\cdots\right) r\,d\xi\,d\eta\,|J| \quad (20b)$$

where, k in this case is $k = \sqrt{1-\left(\frac{(\bar{\varepsilon}_r-\bar{\varepsilon}_\theta)}{\bar{\gamma}_{\theta r}}\right)^2}$.

This equation is also easy to compute using Gauss quadrature.

3.2 FE evaluation of the mobilized shear strength, M_C and N_C

Displacements and stresses around a rigid disc, that has either perfectly smooth or perfectly rough interfaces with the surrounding medium, have been established in the past, see for example (Baguelin *et al*. 1977, Amar Bouzid and Vermeer 2009). Unfortunately, displacements in both analytical and numerical analyses were found to be model size dependent. However, it is quite unrealistic that when the outside model radius R_m increases towards infinity, the displacements tend similarly to infinity. Consequently, there are infinite values for N_C and M_C (see Fig. 2 for the definition) as they rely upon displacements.

As far as finding rational values for N_C and M_C is concerned, it necessary to find a reasonable boundary distance which allows to determine unique values for these coefficients. Using upper bound theorem, the boundary which corresponds to lowest N_C can be considered as the effective zone of influence and consequently N_C and M_C can be estimated for this soil boundary. The value of M_C depends essentially on the value of the Mobilised Shear Strain given by Eqs. (16) or (20b). Once the latter is computed, M_C will be easily calculated by the following equation, which is

$$M_C = \varepsilon_{s,mob} \frac{D}{y} \tag{21}$$

The loading acting on the pile can be associated with the mobilized shear strength

$$p = DN_C \tau_{mob} \tag{22}$$

where, N_C is a capacity coefficient and τ_{mob} is the mobilised shear strength. N_C normally referred to as lateral bearing capacity factor in pile foundation design.

Starting from the basic idea that the total strain energy in the system is equal to the work done by external agencies, and the mobilized shear strength is related to the mobilized shear strain by the shear modulus G, one can write

$$\frac{1}{2} py = U \tag{23}$$

and

$$\tau_{mob} = G\varepsilon_{s,mob} \tag{24}$$

where, $G = E/2(1+v)$.

Substituting Eqs. (23) and (24) in Eq. (22), the expression for N_C will have the following form

$$N_c = \frac{2U}{y\, D\, G\, \varepsilon_{s,mob}} \tag{25}$$

Unlike the parameter M_C, which depends only on $\varepsilon_{s,mob}$, the bearing capacity factor N_C depends on the mobilized shear strain and the total deformation energy in the system as well, which can be clearly seen in the Eq. (25).

The expression of total strain energy in the deforming soil is given by

$$U = \int \left[\frac{1}{2} (\sigma_r \varepsilon_r + \sigma_z \varepsilon_z + \sigma_\theta \varepsilon_\theta + \tau_{rz} \gamma_{rz} + \tau_{z\theta} \gamma_{z\theta} + \tau_{\theta r} \gamma_{\theta r}) \right] dv \tag{26}$$

As the nodes belonging to the top and bottom boundaries are restrained against vertical movement, the problem becomes a plane strain one. Hence, only, σ_r, σ_θ and $\tau_{\theta r}$ survive in Eq. (26). Consequently, the latter becomes

$$U = \int \left[\frac{1}{2} (\sigma_r \varepsilon_r + \sigma_\theta \varepsilon_\theta + \tau_{\theta r} \gamma_{\theta r}) \right] dv \tag{27}$$

Eq. (27), can be re-written in a more compact form

$$U = \int \left[\frac{1}{2} \varepsilon^T \, D \, \varepsilon \right] dv \tag{28}$$

where, D is the medium elasticity matrix.

By specifying the integral boundaries, the Eq. (28) becomes

$$U = \frac{1}{2} \int_{-1}^{1} \int_{-1}^{1} \int_{-\pi}^{\pi} \varepsilon^T D \, \varepsilon \, r \, d\xi \, d\eta \, d\theta \left| J \right| \tag{29}$$

Furthermore, all terms of the product $\varepsilon^T D \, \varepsilon$ contain either the term $\cos^2\theta$ or $\sin^2\theta$ in their expressions. Hence, the integration with respect to the angular position θ yields the value of π. The Eq. (29) will have the final form

$$U = \frac{\pi}{2} \int_{-1}^{1} \int_{-1}^{1} \bar{\varepsilon}^T D \, \bar{\varepsilon} \, r \, d\xi \, d\eta \left| J \right| \tag{30}$$

where, $\bar{\varepsilon}$ is the strain amplitudes vector.

Now substituting Eq. (30) along with expression that gives the mobilized shear strain [Eq. (16) or Eq. (20b)] in Eq. (25), it is easy to evaluate the bearing capacity factor N_C.

4. Computational experiments

4.1 Mesh adopted, FE characteristics and computed results

Taking advantage of symmetry, only half of the domain was meshed for the 3D semi-analytical FEM study (Fig. 8). The mesh used for the study, depicted in $r-z$ space, is shown in Fig. 8. It consists of a horizontal disc of soil of unit thickness with an external radius of R_m. Eight-noded isoparametric elements were used to model the soil and the rigid disc. To model the loading of the rigid disc, lateral displacements were imposed at all nodes modeling the disc. Special pile-soil interface elements were implemented since this is required for modeling the smoothness and the roughness of the interface separating the disc from the surrounding medium. The boundary conditions imposed on the mesh are:

(a) Nodes at the boundary region *bc* of the mesh are fixed in all directions.
(b) Nodes on the boundaries *ab* and *dc* are prevented from moving vertically. Consequently, we are confined in this study to a problem in which no separation can occur.

Semi-analytical finite element computations have been carried out in an elastic, isotropic soil characterized by parameters presented in Table 1. The deformation characteristics of the rigid disc have been taken as $E_d = 10^{10}$ kN/m^2 and $v_d = 0.25$ for Young's modulus and Poisson's ratio respectively.

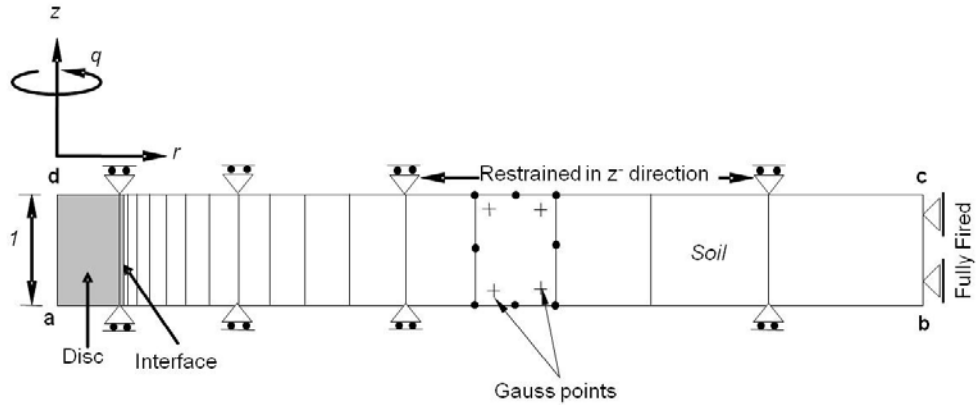

Fig. 8 Mesh used in the semi-analytical FE computation

Table 1 Soil and disc characteristics used in the semi-analytical FE computations

Item	Symbol	Value
Disc diameter	D	1.0 m
Young's modulus of disc	E_d	10^{10} kN/m^2
Poisson's ratio of disc	v_d	0.25
Young's modulus of soil	E_s	100000 kN/m^2
Poisson's ratio of soil	v_s	0.499
Slice thickness	T	1.0 m

Table 2 N_c and M_c values as obtained from the semi-analytical FE computations

Boundary (R_m / r_d)	N_C		M_C	
	Smooth interface	Rough interface	Smooth interface	Rough interface
1.5	13.96	28.26	12.13	18.54
2.0	11.26	19.84	4.33	6.45
2.25	11.23	18.66	3.15	4.60
2.50	11.48	18.09	2.44	3.50
2.75	11.86	17.89	1.97	2.79
2.85	12.04	17.86	1.83	2.59
3.0	12.34	17.90	1.65	2.29
4.0	14.46	19.11	0.95	1.28
5.0	17.19	21.10	0.65	0.86
6.0	19.83	23.39	0.49	0.63
7.0	22.50	25.83	0.38	0.49
8.0	25.19	28.35	0.31	0.39
9.0	27.90	30.93	0.26	0.33
10.0	30.61	33.55	0.23	0.28

The rough interface between the rigid disc and the surrounding medium has been simulated by either prescribing large values for the interface stiffness coefficients ($k_n = 10^{12}$ kN/m^3 and $k_s = 10^{12}$ kN/m^3) or fully removing the interface formulation from the FE code by using a conventional analysis in which soil and disc are tied together at the shared nodes. For simulating a smooth interface, finite element analyses were carried out by imposing a shear stiffness of $k_s = 0.0$ and a large value for the normal stiffness, $k_n = 10^{12}$ kN/m^3. The displacement applied to the inner disc (i.e., modelled pile) was 0.001 m.

The solutions for N_C and M_C for different outer rigid boundaries of the soil are plotted in Fig. 9 and are presented in Table 2. Fig. 9(b) shows the non convergence of M_C with outer boundary. This aspect is also reported in the literature, see for example (Baguelin *et al*. 1977, Chaudhry 1994). This is may be due to the fact that a 3D problem is being simulated in a 2D. Also the load dispersion is not taken into account.

Considering that the velocity field is proportional to the displacement field, the upper bound solution can be sought for the optimal extent of the outer rigid boundary at the lowest occurring value of N_C. The solution, hence, gives the optimal boundary of $2.25r_d$ for the smooth pile-soil interface which increases to $2.85r_d$ for rough interface. The value of M_C corresponding to the optimal boundary is 3.15 for smooth interface and 2.59 for rough interface.

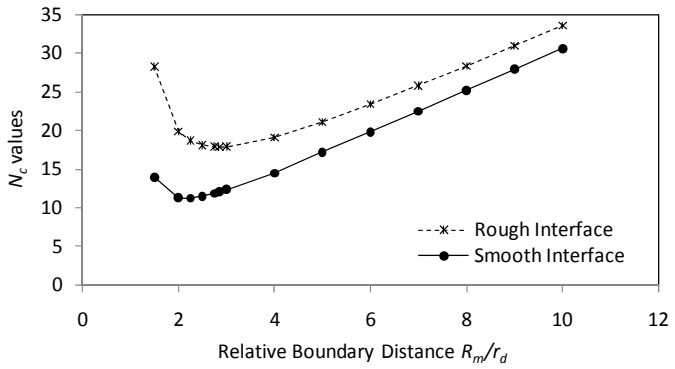

(a)

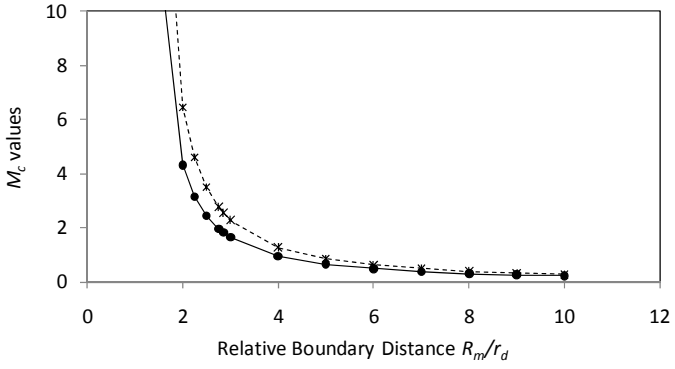

(b)

Fig. 9 (a) N_C and (b) M_C values for a nearly incompressible elastic soil for different outer rigid boundaries, $R_m = 1.5r_d$ to $10r_d$

4.2 Comparison of semi-analytical FE solution with other numerical and analytical procedures

To verify the above Semi-Analytical FE results, the solution is repeated with a complete numerical FE model using COMSOL Multiphysics® (COMSOL 2009). A 2D pile-soil interaction was modelled in a plane strain environment. Mesh optimization, parametric study and model verification were performed before analyzing the pile-soil problem. The material was modelled as linear elastic with a non-slip boundary with the pile (which corresponds to a rough pile-soil interface). The exterior boundary was fixed, and a defined displacement was applied on the outer surface of the pile. A triangular mesh was adopted (Fig. 10(a)) with Lagrange-quadratic elements. The material properties assigned to the model were as specified in Table 1. The pile deflection was modeled as rigid displacement of the inner boundary.

As described in Section 3.2, the value of N_C and M_C are based on the mobilized strain in the deformation field. In the FE model, the mobilized strain was calculated by averaging the engineering strain over the entire volume of the soil considered as given in Eq. (9). The boundary corresponding to the lowest value of N_C was considered as the effective zone of influence and the single representative value of N_C and M_C were obtained. Fig. 10(b) plots the strain (engineering shear strain) field due to the displacement of inner boundaries and the displacement vectors for a representative boundary zone where $R_m = 2.85r_p$. As expected higher shear strains are observed orthogonal to the displacement vector and a flow around mechanism is apparent.

Using Eqs. (9), (21) and (25), the N_C and M_C values were obtained from the FE solution for different soil boundary zones. These values were then compared with the Semi-analytical FE solution described in Section 3.2 and are shown in Figs. 11 and 12. In addition to FE results carried out in this study, solutions by Einav and Randolph (2005) and Martin and Randolph (2006) are also included in the figures for comparison. Einav and Randolph used an upper bound solution

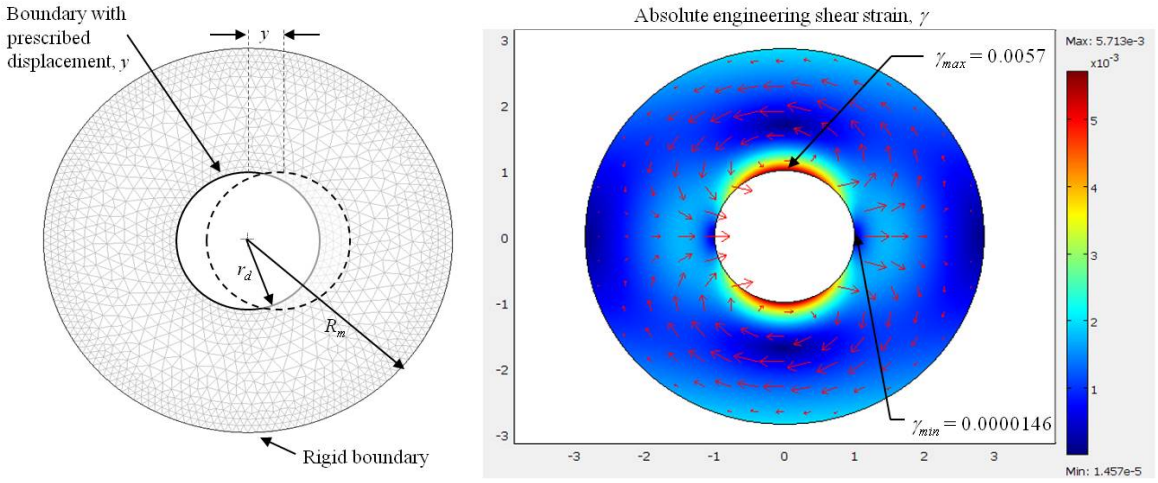

(a) (b)

Fig. 10 (a) Pile-soil interaction mesh in numerical FE model in COMSOL; (b) Elastic strain field due to inner rigid disk displacement of 0.001 m for nearly incompressible soil (Extent of rigid soil boundary, $R_m = 2.85r_p$)

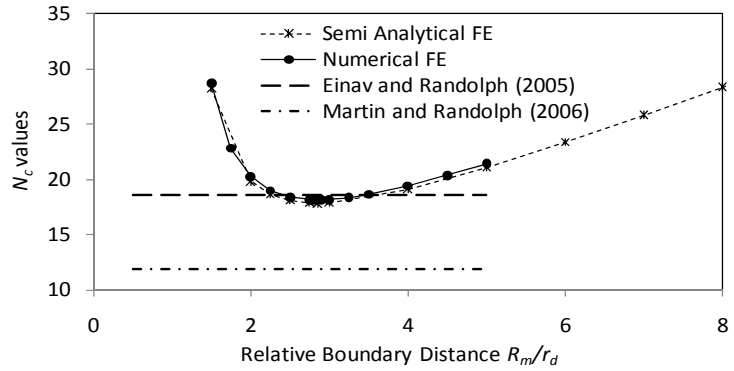

Fig. 11 Comparison of N_C values obtained by different solutions for different outer rigid boundaries, $R_m = 1.5r_d$ to $8r_d$

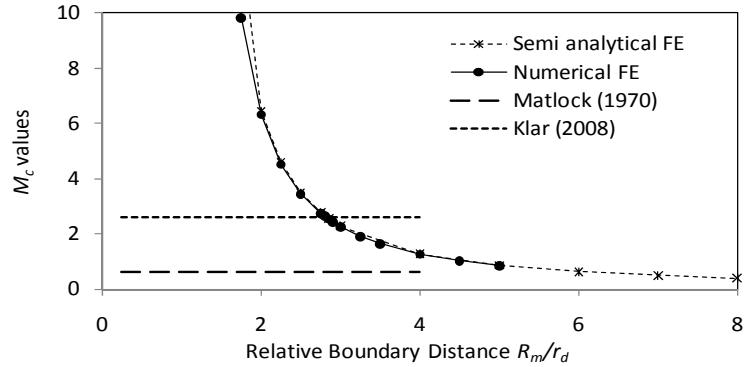

Fig. 12 Comparison of M_C values obtained by different solutions for different outer rigid boundaries, $R_m = 1.5r_d$ to $8r_d$

Table 3 Summarizes the results of M_C and N_C from the analysis presented in this paper which will be used in the next section for the construction of the *p-y* curves

	M_C	N_C
Linear elastic soil with smooth interface	3.15	11.23
Linear elastic soil with rough interface	2.59	17.89
Rigid plastic with rough interface	2.60	9.00

using the method of strain path in the flow field derived from classical fluid mechanics theories with strain softening behavior of an incompressible material. However, Martin and Randolph employed an upper bound plasticity solution for a perfectly plastic material. Four important points are worth noting from the examination of these figures:

(a) A perfect agreement is observed between the semi-analytical FE results and those of conventional FE solutions provided by COMSOL for the entire range of the relative boundary distances considered.

(b) For both analyses the lowest value of N_C which is approximately 17.86 occurs at the same relative boundary distance $R_m/r_d = 2.85$.
(c) FE results are in very close agreement with the solution provided by Einav and Randolph.
(d) Solutions by Martin and Randolph is lower than the other results, which is probably due to the consideration of a perfectly plastic material.

Comparisons of M_C values between semi-analytical FE solutions, COMSOL results and those of other methods reported in the literature are illustrated in Fig. 12. At the first sight, Fig. 12 shows a perfect agreement between the semi-analytical FE solutions and COMSOL results. If we consider as effective influence zone the relative boundary distance at which the lowest value of N_C occurred ($R_m/r_d = 2.85$ in Fig. 11) both analyses provided the nearly same value of $M_c = 2.59$. This is in very close agreement with the solution by Klar (2008).

5. Example of constructing *p-y* curve from stress-strain curve using M_C and N_C values

This section of the paper demonstrates the application of MSD concept for the construction of *p-y* curve from stress-strain of the soil shown in Fig. 3. M_C and N_C values were obtained for both smooth pile-soil interface and rough pile-soil interface for elastic medium. M_C and N_C thus obtained are 3.15 and 11.23 for smooth interface and 2.59 and 17.89 for rough interface. As these values are obtained for an elastic medium, they can be used to scale stress-strain curve to *p-y* curve till elastic zone. The solution for fully plastic condition, i.e., $M_C = 2.6$ (Matlock 1970) and $N_C = 9$ (Randolph and Houlsby 1984) may be used after the occurrence of maximum shear stress. However if the changeover of N_C or M_C happens abruptly, there will also be abrupt change in the shape of *p-y* curve, which must be avoided for convergence of numerical solution.

The proposed scheme is therefore to assume that the soil is elastic till half of the maximum shear stress where N_C can be taken as 11.23 (smooth interface) or 17.86 (rough interface).

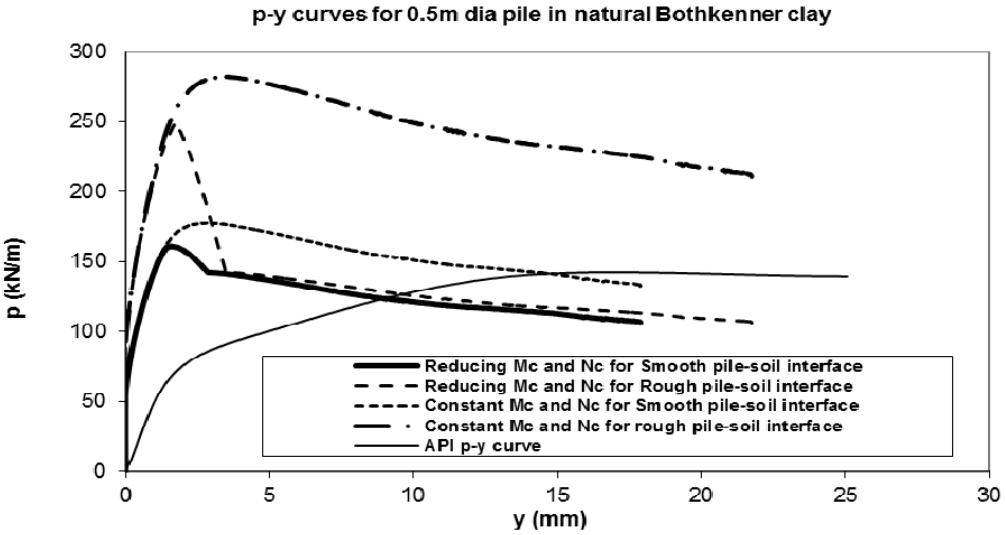

Fig. 13 Construction of *p-y* curves using different methods

Subsequently, N_C can be gradually reduced to 9 from half the shear stress to the maximum shear stress. After the maximum shear stress is reached, N_C can be kept constant as 9 for rest of the stress values. M_C can be conveniently taken as 2.6 throughout the range. Fig. 13 shows five *p-y* curves for a concrete pile of diameter 0.5 m. Two simplified *p-y* curves, for smooth and rough pile-soil interface, using constant values of M_C and N_C throughout the scaling of stress-strain is constructed. The *p-y* curve as suggested by API guidelines was also prepared for comparison, which does not distinguish between smooth or rough pile-soil interfaces.

To demonstrate the effect of different *p-y* curve as constructed above in pile response, a numerical study is carried out for a concrete pile of 0.5 m diameter and 30 m long embedded in uniform Bothkennar clay. For the pile, the grade of concrete is considered to be 4000 psi (F_{ck} = 30 MPa) and the grade of steel reinforcement is ASTM A615 Grade 60 (F_y = 420 MPa). The pile is reinforced with 8 longitudinal bars of 14 mm diameter and lateral ties of 6 mm diameter at a spacing of 150 mm. This exercise has some limitations in the sense that while uniform clay throughout the depth may be possible but this *p-y* curve (which is suited for a deeper depth) may be unrealistic in the top part of the pile due to the wedge mechanism that develops. However, this numerical exercise is carried out to demonstrate the effect of the shape of the *p-y* curve and therefore the use of the same *p-y* curve is considered throughout the depth. The *p-y* curves are assigned as the backbone load-deformation curve for soil springs lumped at 0.25 m interval all along the height of the pile. The schematic of the numerical model is shown in the Fig. 14. A lateral load was applied at the pile top and this load was increased gradually which is similar to the push-over type of analysis. The load-deflection pattern of the pile head thus obtained for different *p-y* curves is plotted in the Fig. 15 below. Few points may be noted:

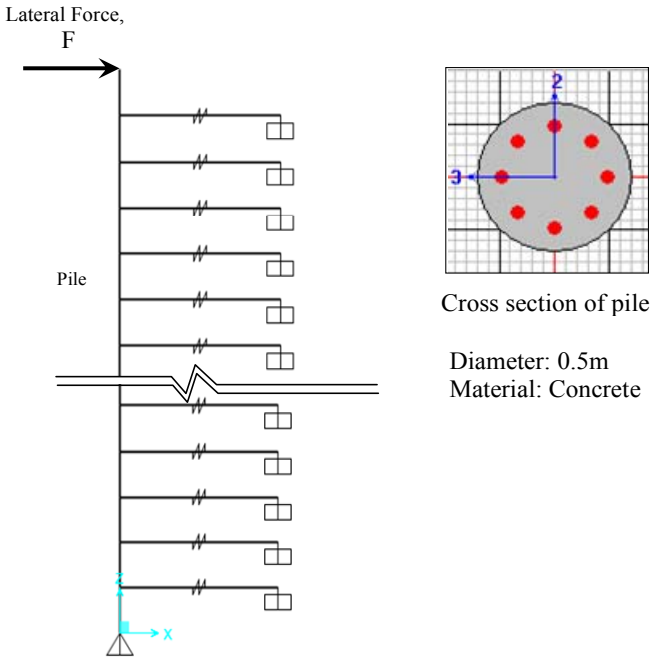

Fig. 14 SAP model of the pile

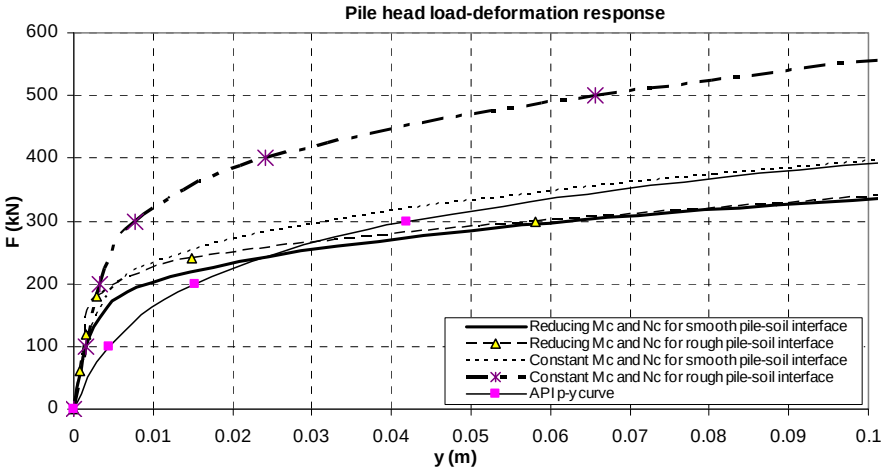

Fig. 15 Lateral load versus pile head deflection for different types of *p-y* curves

(a) Ultimate load capacity is similar for the three *p-y* curves (API and the proposed ones with reduced M_C and N_C) for pile head deflection of 5% of pile diameter i.e., 25 mm. The *p-y* curves with constant M_C and N_C values over predict the ultimate load capacity.

(b) The slope of the lateral load–pile head deflection curve provides an estimate of the pile head stiffness and these values are necessary for carrying out dynamic analysis of various structures i.e., monopile supported wind turbines. Fig. 15 suggests that API underestimates the pile head stiffness. While this can be viewed as conservative for predicting deformation of the foundation but this may predict lower natural frequency of a pile-supported structure.

6. Conclusions

A method is proposed to construct a continuous *p-y* curve for a pile from stress-strain data of a representative soil. The proposed method has the advantage of retaining most of the features of stress-strain relationship. This is in contrast to the commonly used method of construction where two values are taken from a stress-strain data (undrained strength and the strain at 50% of the failure stress) to construct the *p-y* curve. The method is based on MSD (Mobilized Strength Design) concept where the stress-strain axis is scaled differently to obtain the *p-y* curve. The stress axis is scaled using N_C to obtain *p* and the strain axis is scaled using a factor M_C to obtain y.

Potentially, a three-dimensional finite element analysis could be used to analyze most complicated soil/structure interaction problems. However, analysis of such problems usually demands the discretization of the continuum in all three dimensions leading to very large sets of algebraic equations to solve and requiring a substantial human effort to process data. As an alternative, a semi-analytical FE approach is used to get the scaling factors M_C and N_C where the quantities of interest are expanded in Fourier series. Both smooth and rough interfaces were considered. Semi-Analytical FE results for a rough disc were found to be in good agreement with those of other numerical and analytical procedures.

The presented problem has both a practical and a theoretical significance in geotechnical engineering. The theoretical significance is obvious and the practical significance is that the present approach gives the engineers a strong tool to derive *p-y* curves from their experimentally established soil stress-strain relationships. This may provide a better prediction of pile head stiffness required for dynamic analyses and deformation under working loads.

Acknowledgements

The authors would like to thank Dr. David Nash of Department of Civil Engineering, University of Bristol, for providing the accurate stress-strain relationships of Bothkennar clay.

References

Adhikari, S. and Bhattacharya, S. (2011), "Vibrations of wind-turbines considering soil-structure interaction", *Wind Struct. Int. J.*, **14**(2), 85-112.

Amar Bouzid, Dj. (2011), "Finite element analysis of a piled footing under horizontal loading", *Geomech. Eng. Int. J.*, **3**(1), 29-43.

Amar Bouzid, Dj. and Vermeer, P.A. (2009), "Fourier series based FE analysis of a disc under prescribed displacements-elastic stress study", *Arch. Appl. Mech.*, **79**(10), 927-937.

Amar Bouzid, Dj., Tiliouine, B. and Vermeer, P.A. (2004), "Exact formulation of interface stiffness matrix for axisymmetric bodies under non-axisymmetric loading", *Comput. Geotech.*, **31**(2), 75-87.

American Petroleum Institute (API) (2001), *Recommended Practice for Planning Designing and Constructing Fixed Offshore Platforms – Load and Resistance Factor design*, 21st Edition.

Baguelin, F., Frank, R. and Said, Y.H. (1977), "Theoretical study of lateral reaction mechanism of piles", *Géotech.*, **27**(3), 405-434.

Bolton, M.D. (2012), *Performance-Based Design in Geotechnical Engineering*, 52nd Rankine Lecture, ICE, Paper to appear in Géotechnique.

Bouafia, A. (2007), "Single piles under horizontal loads in sand: determination of P-Y curves from the prebored pressuremeter test", *Geotech. Geol. Eng.*, **25**(3), 283-301.

Bowles, J.E. (1996), *Foundation Analysis and Design*, 4th Edition, McGraw-Hill, London.

Byrd, P.F. and Friedman, M.D. (1971), *Handbook of Elliptic Integrals for Engineers and Scientists*, 2nd Edition, Springer-Verlag, New York.

Chaudhry, A.R. (1994), "Static pile-soil-pile interaction in offshore pile groups", Ph.D. Thesis, University of Oxford, UK.

COMSOL multiphysics user guide (2009), Version - 3.5a Edition, COMSOL AB Stockholm, Sweden.

Cook, R.D., Malkus, D.S., Plesha, M.E. and Witt, R.J. (2001), *Concepts and Applications of Finite Element Analysis*, 4th Edition, Wiley, New York.

Cox, W.R., Reese, L.C. and Grubbs, B.R. (1974), "Field testing of laterally loaded piles in sand", *Proceedings 6th Offshore Technology Conference*, Houston, Texas, 459-472.

Dash, S.R., Bhattacharya, S., Blackborough, A. and Hyodo, M. (2008), "P-Y curve to model lateral response of pile foundations in liquefied soils " *The 14th World Conference on Earthquake Engineering*, Beijing, China, October.

DNV (2001), *Guidelines for Design of Wind Turbines*, Publication from DNV/Riso in technical co-operation.

Einav, I. and Randolph, M.F. (2005), "Combining upper bound and strain path methods for evaluating penetration resistance", *Int. J. Numer. Method. Eng.*, **63**(14), 1991-2016.

Frank, R. (2009), "Design of foundations in Trance with the use of Menard pressuremeter tests (MPM)", *Soil Foundation Eng.*, **46**(6), 219-231.

Hajialilue-Bonab, M., Azarnya-Shahgoli, H. and Sojoudi, Y. (2011), "Soil deformation pattern around laterally loaded piles", *Int. J. Phys. Model. Geotech.*, **11**(3), 116-125.
Klar, A. (2008), "Upper bound for cylinder movement using elastic fields and its possible application to pile deformation analysis", *Int. J. Geomech.*, **8**(2), 162-167.
Martin, C.M. and Randolph, M.F. (2006), "Upper bound analysis of lateral pile capacity in cohesive soil", *Géotech.*, **56**(2), 141-145.
Matlock, H. (1970), "Correlation for design of laterally loaded piles in soft clay", *Offshore Technology Conference*, Houston, Texas, USA, April.
McClelland, B. and Focht, J.A.J. (1958), "Soil modulus for laterally loaded piles", *Transactions*, *ASCE*, **123**(1), 1049-1063.
Osman, A.S. and Bolton, M.D. (2005), "Simple plasticity-based prediction of the undrained settlelment of shallow circular foundations on clay", *Géotech.*, **55**(6), 435-447.
Randoph, M.F. and Houslby, G.T. (1984), "The limiting pressure on a circular pile loaded laterally in cohesive soil", *Géotech.*, **34**(4), 613-623.
Reese, L.C. and Impe, W.F.V. (2001), *Single Piles and Pile Groups under Lateral Loading*, A.A. Balkema Publishers, Brookfield.
Reese, L.C., Cox, W.R. and Koop, F.D. (1974), "Analysis of laterally loaded piles in sand", *Proceedings of 6th Offshore Technology Conference*, Houston, Texas, 473-483.
Reese, L.C., Wang, S.T., Isenhower, W.M. and Arrellaga, J.A. (2000), *Computer Program LPILE Plus Version 4.0 Technical Manual*, Ensoft, Inc., Austin, Texas.
Zienkiewicz, O.C. and Taylor, R.L. (1991), *The Finite Element Method*, 4th Edition, McGraw-Hill, London.

PL